RSC Advances

Electrochemical assessment of phenol and triazoles derived from phenol (BPT) on API 5L X52 steel immersed in 1M HCl

Journal:	*RSC Advances*
Manuscript ID	RA-ART-04-2016-009832.R1
Article Type:	Paper
Date Submitted by the Author:	10-Jul-2016
Complete List of Authors:	Espinoza-Vázquez, Araceli; Universidad Nacional Autonoma de Mexico, Department of Metallurgical Engineering Rodríguez Gómez, Francisco; Universidad Nacional Autonoma de Mexico, Department of Metallurgical Engineering González-Olvera, Rodrigo; Universidad Autónoma Metropolitana-Azcapotzalco, Ciencias Básicas Angeles-Beltrán, Deyanira; Universidad Autónoma Metropolitana, Departamento de Ciencias Básicas Mendoza-Espinosa, Daniel; Universidad Autónoma Metropolitana-Azcapotzalco, Ciencias Básicas Negrón-Silva, Guillermo; Universidad Autónoma Metropolitana, Departamento de Ciencias Básicas
Subject area & keyword:	Electrochemistry < Physical

RSC Advances

ARTICLE

Electrochemical assessment of phenol and triazoles derived from phenol (BPT) on API 5L X52 steel immersed in 1M HCl

Received 00th January 20xx,
Accepted 00th January 20xx

DOI: 10.1039/x0xx00000x

www.rsc.org/

A. Espinoza-Vázquez, [a] F. J. Rodríguez-Gómez, [a] R. González-Olvera, [b] D. Angeles-Beltrán, [b] D. Mendoza-Espinosa, [b] and G. E. Negrón-Silva[b,] *

The corrosion inhibition of phenol triazoles was tested with several halogens by means of electrochemical impedance and potentiodynamic polarization. We observed the importance of the 1,2,3-triazole ring in the chemical structure because significant inhibition efficiencies (η) > 90% were achieved at low concentrations with the different halogens. These compounds have a physisorption-type adsorption process, in accordance with the Langmuir model. For long immersion times, the organic inhibitor BPTI showed good corrosion protection during 504 hours of immersion with η > 80%. Furthermore, the hydrodynamic conditions proved that organic molecules experience a desorption process related to the different rotation velocities employed. Finally, it was demonstrated by SEM that the corrosion velocity is diminished when using the BPTI inhibitor at 50 ppm.

Introduction

Corrosion occurs as metals are oxidised when they get immersed in a corrosive environment, for example, in the presence of oxygen, H_2S, and so on, resulting in the formation of stable solids. Acids such as HCl and H_2SO_4 are widely used in metal pickling as decalcification and cleansing agents in several industries for the elimination of oxide layers and unwanted corrosion by-products[1-3]. Several methods can be used to diagnose, evaluate, and control corrosion issues. An alternative to solve this problem is the use of corrosion inhibitors [4-10].

Corrosion inhibitors cause the formation of protective layers in pipelines. Although these layers reduce corrosion, they are unable to counteract it entirely. Generally, organic inhibitor adsorption is affected by various factors such as the electronic distribution, nature of the metal, chemical structure, and corrosive medium [11-14].

In the oil industry, carbon steel used to convey hydrocarbons is exposed to aggressive fluids [15], and this exposure decreases with organic corrosion inhibitors[16-20]. During transport, molecules interact causing several transfer phenomena (momentum, mass, heat, and so on). Under certain circumstances, fluid movement can be described as the displacement of a set of molecular layers sliding one over the other. In these conditions, it is assumed that the molecules belonging to a particular layer do not move to another layer, that is, there is no mixing. This movement without mixing is called "laminar flow" [21-22].

It has been demonstrated that organic compounds such as 1,2,3-triazoles derived from carbohydrates, amino acids, maleic acid and chalcones, among other organic compounds, are efficient steel acid corrosion inhibitors (Fig. 1) [23-28]. Copper(I) catalysed 1,3-dipolar cycle-addition (also known as Click's reaction or Huisgen-Meldal-Sharpless's reaction) is the most versatile synthetic strategy for 1,4-disubstituted 1,2,3-triazoles from azides and terminal alkynes [29-30]. This reaction allowed the preparation of a variety of compounds that contain the 1,2,3-triazole heterocycle. In this regard, our group has synthesised and assessed the inhibitory activity on acid corrosion from the 1,2,3-triazoles of the nucleobases uracil and thyamine [31-33], 2-mercaptobenzimidazole[34] and 3,4-dihydropyrimidinones[35]. Carrying on with our research on organic corrosion inhibitors, here we report the assessment of the inhibitory activity of phenol and its derivatives, which incorporate the 1,2,3-triazole heterocycle, by means of potentiodynamic polarisation, electrochemical impedance spectroscopy, and scanning electron microscopy (SEM).

Experimental

Synthesis

The (prop-2-ynyloxy)benzene **2** and the triazoles 1-benzyl-4-phenoxymethyl-1*H*-1,2,3-triazole (BPT) (**3**), 1-(4-fluorobenzyl)-4-phenoxymethyl-1*H*-1,2,3-triazole (BPTF) (**4**), 1-(4-bromobenzyl)-4-phenoxymethyl-1*H*-1,2,3-triazole (BPTBr) (**6**) and 1-(4-iodobenzyl)-4-phenoxymethyl-1*H*-1,2,3-triazole (BPTI) (**7**) were synthesised according to a modification of our previously reported methodology. The 1-(4-chlorobenzyl)-4-phenoxymethyl-1*H*-1,2,3-triazole **5** (BPTCl) was also synthesised according to our previously reported methodology [31-36]. The molecular structures of compounds

[a] *Department of Metallurgical Engineering, School of Chemistry, Universidad Nacional Autónoma de México, Av. Universidad No. 3000, Coyoacán, C.U., C.P. 04510, Ciudad de México, México.*
[b] *Department of Basic Science, Universidad Autónoma Metropolitana-Azcapotzalco., Av. San Pablo No.180, C.P. 02200, Ciudad de México, México*
** Corresponding author E-mail address: gns@correo.azc.uam.mx (G.E.N.-S)*
Electronic Supplementary Information (ESI) available: [details of any supplementary information available should be included here]. See DOI: 10.1039/x0xx00000x

2-7 are shown in Fig. 2. The structures and purities of all of the synthesised compounds were confirmed by ^{1}H and ^{13}C NMR. The ^{1}H and ^{13}C NMR spectral profiles for these compounds match with what we had previously reported[36].

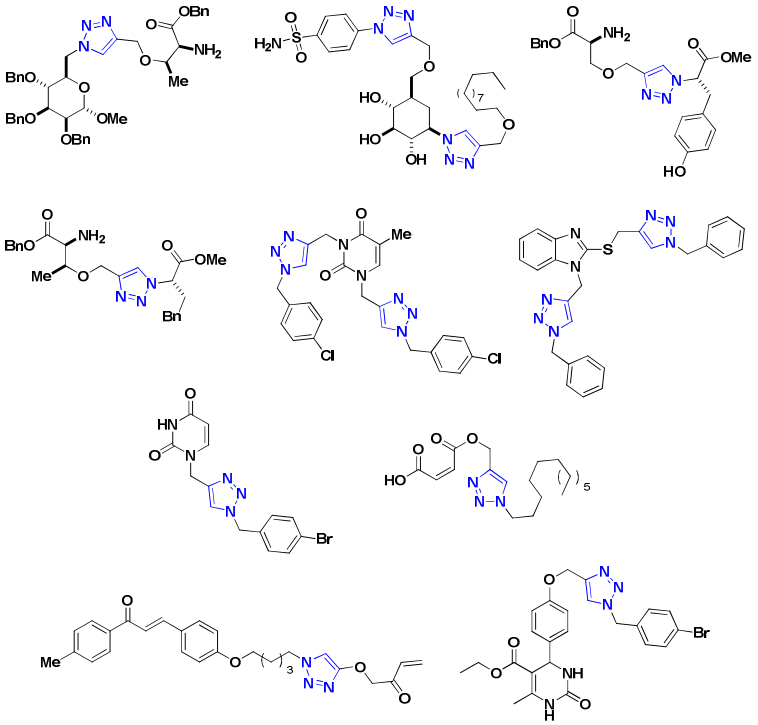

Fig. 1 Organic compounds containing 1,2,3-triazole with acid corrosion inhibitory activity.

Preparation of solutions

Solutions of phenol **1** and its derivatives **2-7** were prepared by dissolving each in DMF. Afterwards, a concentration sweep was carried out from 5 to 200 ppm of the inhibitor in the corrosive 1 M HCl solution.

Electrochemical tests

For the electrochemical impedance spectroscopy (EIS), Gill-AC equipment was used and ±10 mV of sinusoidal potential was applied over a frequency range of 10^{-1} Hz to 10^{4} Hz in a three-electrode electrochemical cell; the working electrode was API 5L X52 steel, the reference electrode was Ag/saturated AgCl, and the counter electrode was graphite.

The hydrodynamic conditions were assessed by means of a rotator disk (PINE Research Instrumentation, AFMSRCE model) at different rotation velocities, such as 300 and 600 rpm, based on the compound that had better inhibition efficiency under static conditions.

The electrode surface, presenting an exposed area of 0.196 cm^2, was prepared using a conventional metallographic method, which involves grinding with sandpaper of grain 80, 120, 240, 320, 400, 600, 1000 and 1200. Subsequently, the surface was polished with 0.3 μ alumina until it was mirror-finished. Then, a water wash was performed, a few millilitres of acetone was added, and finally the surface was thoroughly dried with compressed air so it could be used in the different electrochemical tests.

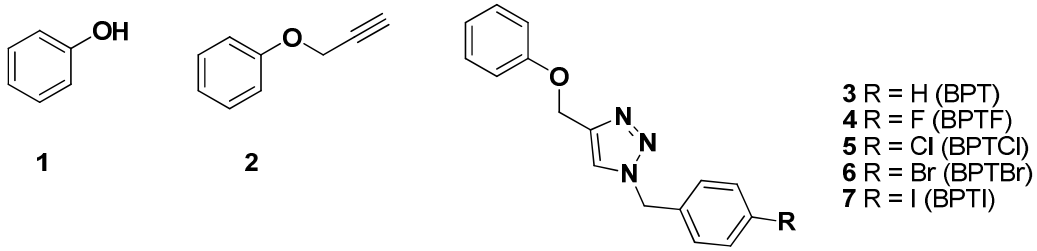

Fig. 2 Chemical structures of the compounds assayed as corrosion inhibitors.

Additionally, an assessment of the immersion time of the best compound at its optimal concentration (50 ppm) was performed for long time periods, with 30 days being the maximum.

After EIS measurements, the potentiodynamic polarization curves of the best inhibitor, the inhibitor that achieved the highest efficiency value, were plotted. The measurements covered a range of -500 mV to 500 mV regarding the open circuit potential (OCP), with a sweep velocity of 66.07 mV/min using the ACM Analysis software for data interpretation.

Surface characterisation

The API 5L X52 steel surface was prepared both without (blank) and with inhibitor (BPTI); a 50 ppm concentration was used for a 48-h immersion time. After the experiment, the steel was washed with distilled water, dried and surface analysed using a Zeiss SUPRA 55 VP electronic sweep microscope at 10 KV along with a 300 X secondary electron detector.

Results and discussion

Synthesis

The synthesis of alkyne **2** was carried out from phenol **1** and propargyl bromide in presence of potassium *t*-butoxide at reflux with microwave irradiation (MW). The desired product **2** was obtained in an 81% yield after column chromatography purification (Fig. 3).

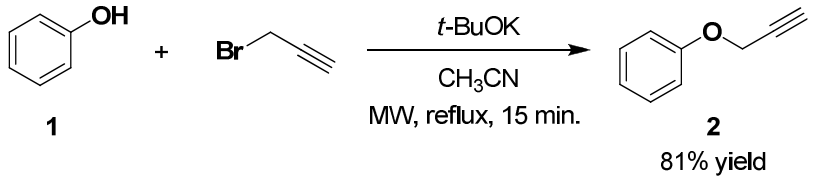

Fig. 3 Microwave-assisted synthesis of 2.

The 1,2,3-triazole derived from phenol **5** was synthesised from a multicomponent reaction involving alkyne **2**, sodium azide and the chloride of the 4-clorobenzyl following our reported methodology [36] (Fig. 4a). The 1,2,3-triazoles derived from phenols **3**, **4**, **6** and **7** were synthesised by the modification of our previously reported methodology. The multicomponent reaction between alkyne **2**, sodium azide and the corresponding benzyl halides was carried out in the presence of monohydrated cupric acetate, monohydrate 1,10-phenanthroline and sodium ascorbate in ethanol-water under heating at 90 °C for 15 minutes with microwave irradiation. The desired triazoles **3**, **4**, **6** and **7** were obtained with good yields after column chromatography purification and recrystallization (Fig. 4b).

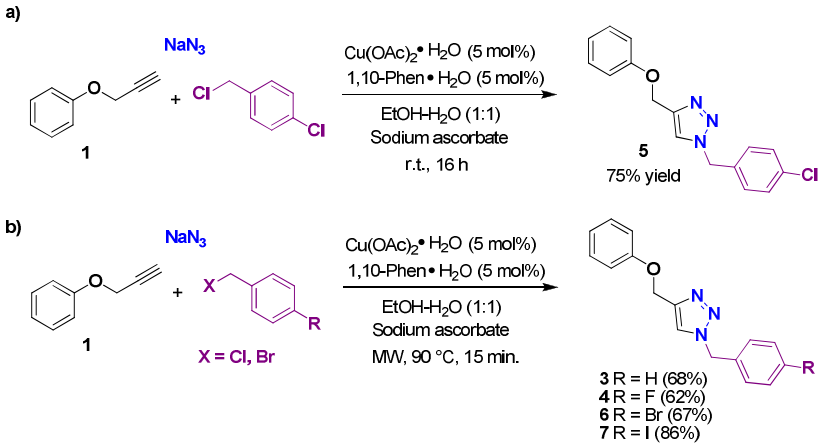

Fig. 4 Multicomponent synthesis for 1,2,3-triazole derivatives of phenol.

Open circuit potential (OCP)

Before carrying out the EIS electrochemical tests and potentiodynamic polarization, an open circuit potential (OCP) stabilisation is needed. Fig. 5 shows some examples of the API 5L X52 electrode OCP variations in time with and without the presence of the 10 ppm of BPT inhibitors. It seems that a stationary state was reached after 500 seconds, and in some cases, the potential becomes even more negative, suggesting that the inhibitor has adhered to the metal surface.

RSC Advances

ARTICLE

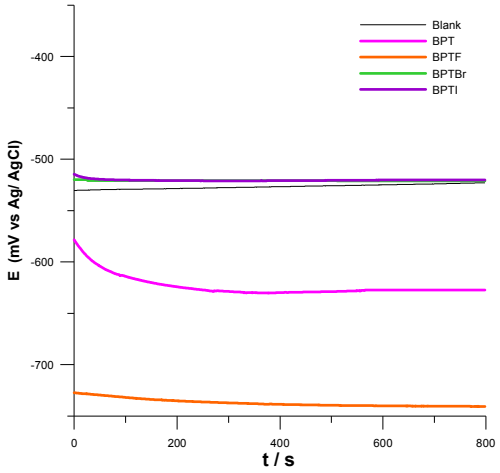

Fig. 5 OCP over time with and without 10 ppm of BPT on API 5L X52steel immersed in 1 M HCl.

EIS measurements

In Fig. 6a, the Nyquist diagram corresponding to the steel immersed in 1 M HCl is shown, and it can be observed that it reached 30 Ω cm^2, and it shows a well-defined semicircle related to the charge transfer resistance. Next, in Fig. 6b, the diagram when different concentrations of the phenol compound are added is shown, and a constant increase in the value of Z_{re} as the inhibitor concentration (225 Ω cm^2) is increased to 200 ppm is observed. In this case, the semicircle formed is depressed, which is attributed to the existence of roughness on the surface [37-38].

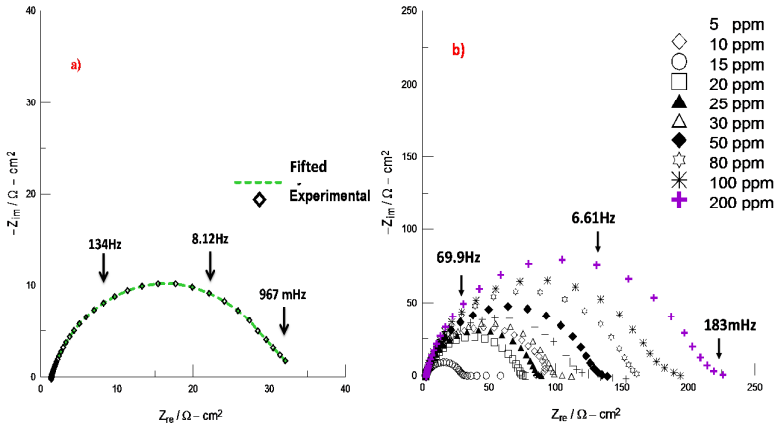

Fig. 6 Nyquist diagrams of API 5L X52 steel immersed in 1 M HCl a) without inhibitor and b) with the presence of phenol.

The propargylated compound of phenol **2** was also evaluated as a corrosion inhibitor, and the same effect was observed; as the concentration increases, the Z_{re} value also increases (see Fig. S1). When the inhibition efficiency of this compound is compared with phenol, at 10 ppm it reached an η of 84% while at 100 ppm it reached 91% (see Fig. S2), indicating that the presence of a triple bond in the chemical structure showed an improvement in the corrosion inhibition (see Annex S).

After observing and analysing the afore-mentioned results, it was decided to evaluate the triazoles derived from phenol to observe the influence that the benzene ring and corresponding halogen

have within the chemical structure. Fig. 7a and 7b show some of the resulting adjustments on the electrochemical impedance with electric circuits, where evidently, the triazoles and halogen present a good match.

On the other hand, Fig. 7c shows the compound without a halogen, where it is observed that at 5 ppm a Z_{re} value of 100 Ω cm^2 was reached, and from 10 ppm to 200 ppm, this value remains practically constant. Additionally, two time constants can be observed: one related to high frequencies with charge transference resistance and the other related to low frequencies with the organic molecule resistance [39-42].

However, when there is the presence of a halogen, such as fluorine (Fig. 7d), a continuous increase in the Z_{re} value can be observed, reaching approximately 520 Ω cm^2 at 200 ppm, which is slightly higher than when the molecule lacks the halogen. In this case, the inhibitor adsorption mechanism changes, as the semicircle shape appears elongated. Therefore, both time constants are coupled together. When the chemical structure contains chloride or bromide atoms in the benzene ring, it shows a gradual Z_{re} value increase, which at 200 ppm reached 620 Ω cm^2 for the chloride compound and approximately 500 Ω cm^2 for the bromide compound.

Finally, the iodine compound was the one with the highest Z_{re} value starting at 30 ppm.

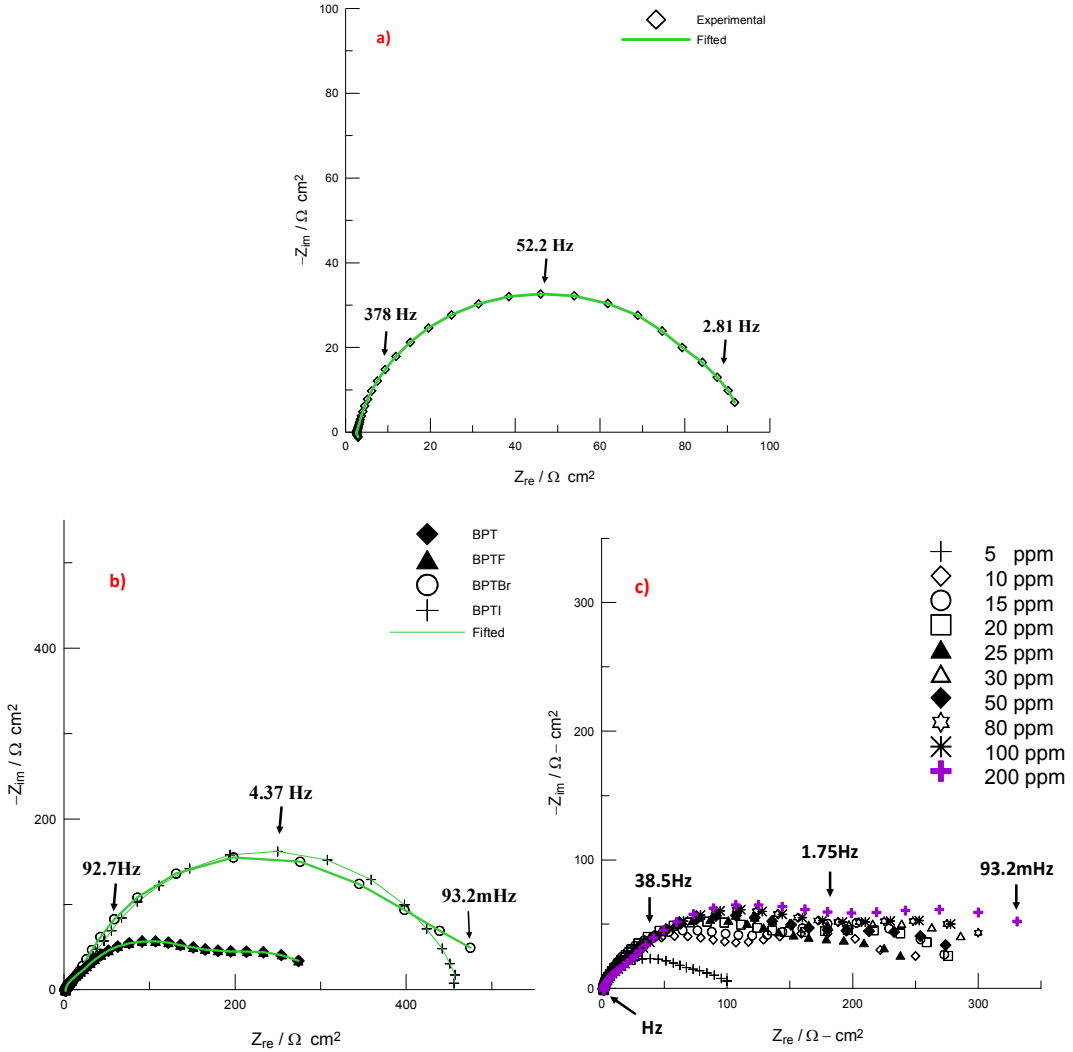

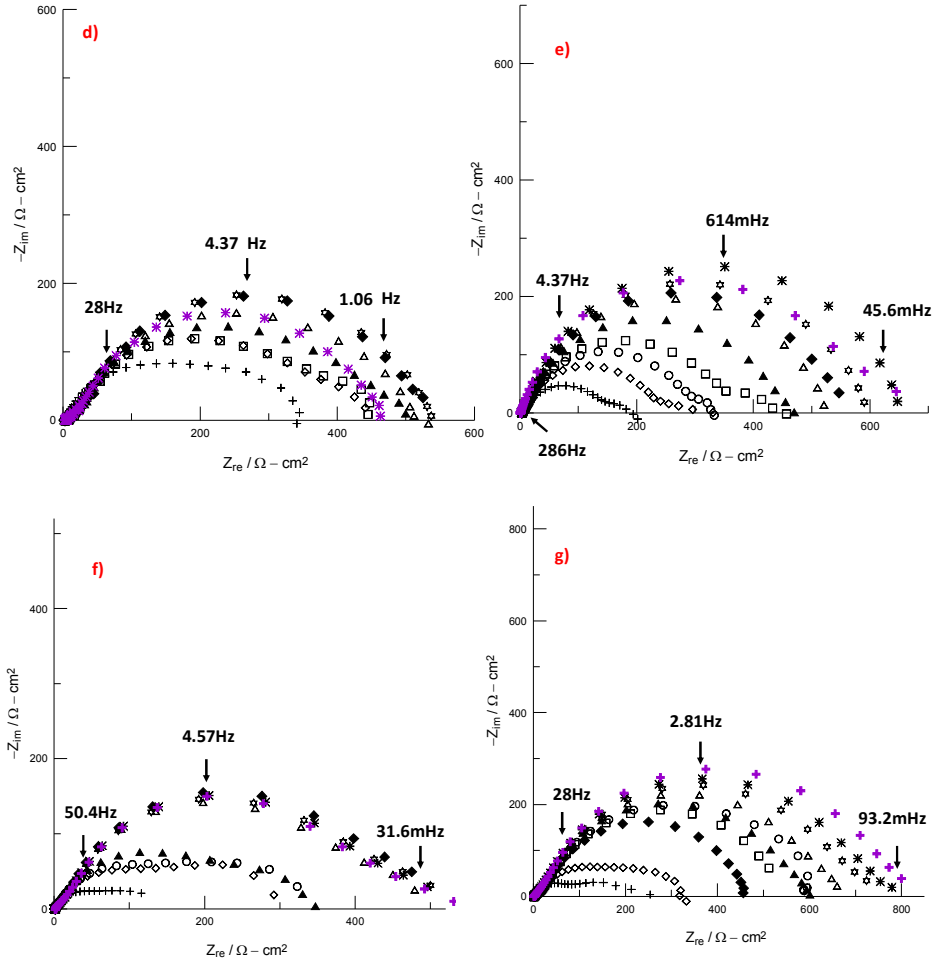

Fig. 7 Nyquist diagrams of API 5L X52 steel immersed in 1 M HCl in presence of: a) phenol simulation, b) phenol derivative simulation, c) BPT, d) BPTF, e) BPTCl, f) BPTBr and g) BPTI.

In Fig. 8, some examples of the bode-phase angle diagrams for API 5L X52 steel with and without 50 ppm of the studied compounds are shown. The increase in the absolute value of impedance |Z| at low frequencies confirms the corrosion protection using these inhibitors because when the inhibitor is added, there is an increase of one order of magnitude. The increase of the phase angle in the presence of the inhibitor indicates that it is adhering to the metallic surface. Additionally, we could clearly observe both time constants for this concentration.

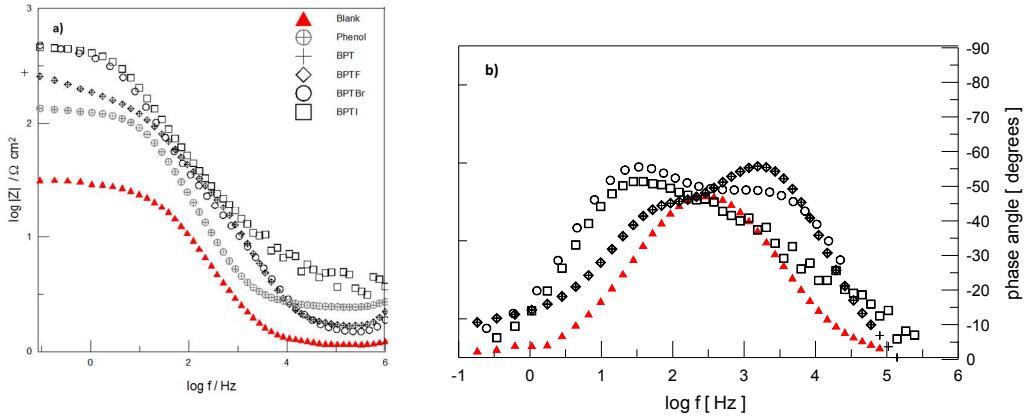

Fig. 8 Bode diagrams for API 5L X52 steel immersed in 1 M HCl with and without 50 ppm of phenol derivatives.

RSC Advances

ARTICLE

The EIS results can be interpreted by means of equivalent electric circuits, as shown in Fig. 9, which were obtained from an open circuit potential with and without the presence of the inhibitor immersed in 1 M HCl [43]. The model corresponding to Fig. 9a is used without the presence of the inhibitor, where R_s is the solution resistance, R_{ct} is the charge transference resistance, and Q is the constant phase element. The model of the electric circuit presented in Fig. 9b is adequate to describe the results in the presence of the inhibitor with the two time constants.

There are also other resistances that allowed the description of the adsorption parameters, such as $R_{mol,}$ which is the resistance of the organic molecules with their corresponding capacitance.

Fig. 9 Equivalent electric circuits used for experimental data adjustments.

Using equation (1), the inhibition efficiency was determined as follows:

$$\eta = \frac{\left(\frac{1}{Rct}\right)blank - \left(\frac{1}{Rct}\right)inhibitor}{\left(\frac{1}{Rct}\right)blank} \; x\; 100 \qquad (1)$$

where R_{ct} is for the absence of an inhibitor and R_{ct} is for the presence of an inhibitor.

For the description of an independent phase displacement of the frequency between an applied potential AC and its current response, a constant phase element (CPE) is used, which is defined in the impedance representation as:

$$\boldsymbol{C_{dl} = Y_0(\omega_m'')^{-n}} \qquad (2)$$

where C_{dl} is the double layer capacitance and ω_m'' is the angular frequency in which Z' is the maximum.

Table 1 shows the phenol electrochemical parameters obtained after the adjustment with the electric circuit. The R_{ct} value increases as the concentrations are increased so the double layer capacitance diminishes, which is attributed to the decrease in the dielectric constant or to the increase in the thickness of the electric double layer due to the phenol adsorption at the metal-solution interface [44].

Table 1 Electrochemical impedance results of phenol as a corrosion inhibitor at different concentrations immersed in 1 M HCl.

Inhibitor	C ppm	R_s Ω cm^2	n	C_{dl} µF cm^{-2}	R_{ct} Ω cm^2	η %
Phenol	0	2.3	0.8	310.0	30.0	-
	10	2.6	0.8	140.9	88.5	66.1
	20	2.3	0.8	158.0	72.3	58.5
	25	2.3	0.8	147.4	84.1	64.3
	30	2.3	0.8	135.3	97.3	69.2
	50	2.5	0.8	122.8	127.7	76.5
	100	2.5	0.8	112.3	175.5	82.9

When the electrochemical parameters of the triazoles derived from phenol were determined (Table 2), it was observed that the second time constant, which is found from the Nyquist and/or Bode diagrams is related to the resistance of the organic molecules [45].

However, the R_{ct} increases at different concentrations with each of the studied inhibitors because the surface coverage increased with increasing concentrations of the organic molecules, and thus, the inhibition efficiency increases [46]. The C_{dl} column decreases as the concentration increases, which is explained by the organic molecules adhering to the API 5L X52 steel surface by displacing the water molecules in the metal-solution interface [47].

Table 2 Electrochemical impedance results of the triazoles derived from phenol as corrosion inhibitors at different concentrations immersed in 1 M HCl.

Inhibitor	C ppm	R_s Ω cm^2	n	C_{dl} μF cm^{-2}	R_{ct} Ω cm^2	R_{mol} Ω cm^2	η %
BPT	5	1.7	0.8	143.7	65.7	44.0	54.3
	10	1.5	0.9	70.1	238.0	70.5	87.4
	20	1.3	0.9	12.0	368.0	-	91.8
	25	1.4	1.0	59.2	235.0	-	87.2
	30	1.4	0.9	70.8	290.7	0.2	89.7
	50	1.7	0.9	15.0	253.9	10.1	88.2
	100	1.9	0.9	16.9	259.2	16.6	88.4
BPTF	5	1.4	1.0	12.9	336.9	5.6	91.1
	10	5.9	1.0	16.9	346.5	78.3	91.3
	20	5.5	1.0	16.3	376.6	62.9	92.0
	25	4.2	0.9	28.6	415.1	64.0	92.8
	30	4.6	1.0	2.5	517.1	10.2	94.2
	50	4.6	0.8	27.4	511.8	25.3	94.1
	100	4.2	0.9	8.5	459.7	13.0	93.5
BPTCl	5	7.2	0.8	109.8	133.9	47.0	77.6
	10	3.5	0.8	112.2	240.7	35.3	87.5
	20	3.3	0.7	108.5	382.0	35.0	92.1
	25	3.4	0.8	58.4	418.8	38.2	92.8
	30	3.4	0.8	72.7	476.0	51.0	93.7
	50	3.3	0.8	82.7	493.0	61.7	93.9
	100	3.4	0.8	75.4	631.0	32.8	95.2
BPTBr	5	1.5	0.8	184.0	141.8	69.6	78.8
	10	1.6	1.0	18.3	276.8	2.6	89.2
	15	1.3	0.3	555.7	488.5	1.3	93.9
	25	1.5	0.9	24.6	312.0	5.9	90.4
	30	1.4	0.8	48.8	415.0	24.3	92.8
	50	1.5	0.8	44.8	444.2	21.0	92.2
	100	1.5	0.8	43.1	438.7	22.5	93.2
BPTI	5	1.9	0.8	121.6	202.8	-	85.2
	10	1.4	1.0	34.2	309.0	-	90.3
	20	1.2	0.8	14.1	557.4	5.0	94.6
	25	1.8	0.7	44.5	601.4	12.0	95.0
	30	1.7	0.7	41.9	683.0	10.6	95.6
	50	3.9	0.7	68.4	469.0	17.4	93.6
	100	1.8	0.7	78.3	764.0	20.1	96.1

In Fig. 10, it can be clearly observed how the presence of the 1,2,3,-triazole ring attached to the phenol compound improves its inhibitory activity against corrosion from low concentrations with η > 90%. Nevertheless, when we compare the triazole derived from phenol without a halogen (BPT) with those that have the halogen bonded to the aromatic ring, the η values of the later improve by

approximately 5%. Accordingly, these inhibitors are fit for the protection of PEMEX ducts.

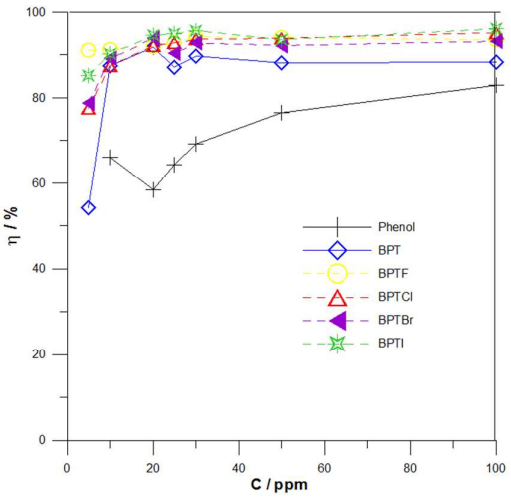

Fig. 10 Inhibition efficiencies of phenol and its derivatives as a function of concentration.

BPTI polarization curves

Tafel polarization curves of API 5L X52 steel at different BPTI concentrations are shown in Fig. 11. The electrochemical parameters obtained in Table 3 are the corrosion potential (E_{corr}), corrosion velocity (i_{corr}), Tafel anodic gradients (βa), Tafel cathodic gradients (βc), and inhibition efficiency (% η).

By means of this technique, we are able to calculate the inhibition efficiency of the organic compound:

$$\eta = (1 - \frac{i_{inhibitor}}{i_{uninhibitor}}) \text{ x } 100 \quad (3)$$

where $i_{inhibitor}$ is the current density with inhibitor and $i_{uninhibited}$ is the current density in the absence of inhibitor.

In Fig. 11 for BPTI under static conditions, it can be observed how the current density decreases in its presence, which suggests that it is retarding the corrosion process due to the protective film formed by the inhibitor on the metallic surface [48].

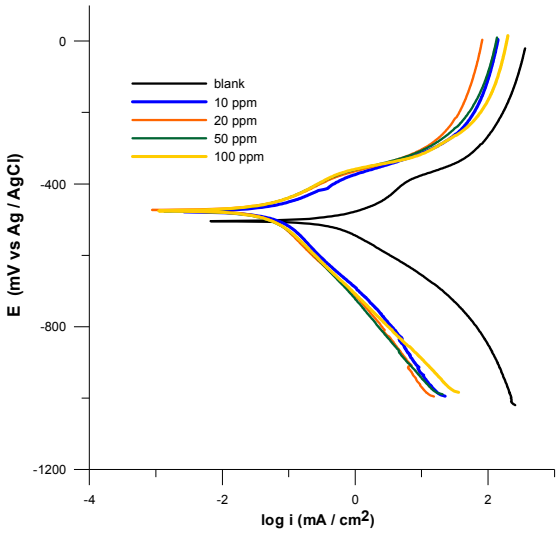

Fig. 11 Potentiodynamic polarisation curves at different BPTI concentrations for API 5L X52 steel immersed in 1 M HCl

The results shown in Table 3 correspond to the corrosion potential (E_{corr}) in the presence of the inhibitor, with the results for the blank being less than 85 mV, which suggests that BPTI is a mixed predominantly anodic type inhibitor [49]. On the other hand, both branches, anodic (βa) and cathodic (βc), show slight changes at the different concentrations studied, which can be attributed to their retardation effects on both anodic and cathodic reactions [50].

RSC Advances

ARTICLE

Table 3 Electrochemical parameters by the potentiodynamic polarization technique for API 5L X52 steel immersed in 1 M HCl in the presence of BPTI.

Inhibitor	C ppm	E_{corr} mV vs Ag /AgCl	I_{corr} mA cm^{-2}	βa mV	βc mV	Θ	η %
BPTI	0	-519.2	0.952	170.2	138.5	-	-
	10	-476.2	0.054	70.5	148.6	0.896	89.6
	20	-468.6	0.010	69.8	88.9	0.942	94.2
	50	-472.8	0.030	64.4	65.2	0.921	92.1
	100	-471.3	0.049	65.8	182.0	0.901	90.1

Adsorption isotherm

After observing that by the electrochemical impedance technique, both phenol and its derivatives provide corrosion inhibition, it is necessary to understand the interactions of these inhibitors with the metallic surface.

To determine the adsorption process, several models (equations 4-7), which describe the behaviour of the organic molecules, are used[51-52]:

$$Ck_{ads} = \frac{\theta}{1-\theta} \quad \textbf{Temkin model} \quad (4)$$

$$\frac{C}{\theta} = \frac{1}{kads} + C \quad \textbf{Langmuir model} \quad (5)$$

$$Ck_{ads^{1/n}} = \theta \quad \textbf{Freundlich model} \quad (6)$$

$$Ck_{ads} = \left(\frac{\theta}{1-\theta}\right) e^{f\theta} \quad \textbf{Frumkin model} \quad (7)$$

where C is the concentration, K_{ads} is the equilibrium constant of the adsorption process, Θ is the coating grade, and 1/n is the constant divided by the adsorbent.

On the other hand, the adsorption equilibrium constant is related to the Gibbs standard free energy, which we can find with equation (8)[53]:

$$\Delta G^{\circ}_{ads} = -RT \ln K_{ads} \quad (8)$$

where R is the ideal gas constant and T is the temperature.

Generally, if ΔG°_{ads} is less than or around -20 kJ/mol, the adsorption process is of the physisorption type because it is associated with the electrostatic interaction between the charge of the inhibitor molecules and the electrode surface charge. However, if this value is -40 kJ/mol or has a more negative value, thus sharing charge or transferring it to the inhibitor molecules on the metal surface by means of coordinated bonds, the process is called chemisorption [54].

After calculating the isotherm with the adsorption models defined by equations 4-7, it was observed that Langmuir model is the best fit, as shown in Fig. 12, because its correlation coefficient is close to 1. This model assumes that the solid surface has a fixed series of adsorption active sites and that each site is occupied by an adsorbed species [55]. From the values calculated using this model, it can be concluded that the adsorption process carried out between the inhibitor and the metallic surface is of the physisorption type (table 4).

RSC Advances

ARTICLE

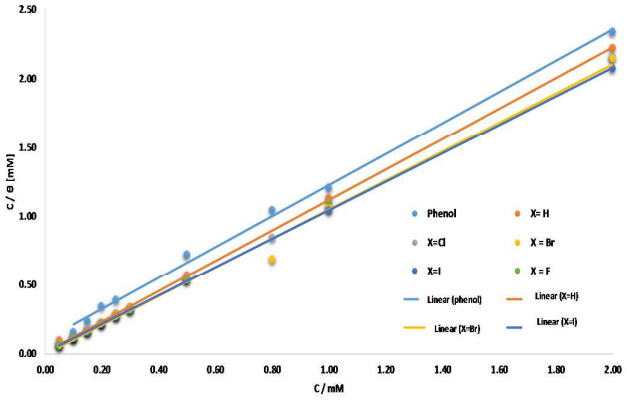

Fig. 12 Langmuir isotherm model adjustment of phenol and its derivatives.

Table 4 Adsorption parameters of the phenol derivatives immersed in 1 M HCl.

Inhibitors	Ln k_{ads}	$\Delta G°_{ads}$ kJmol^{-1}
Phenol	2.32	-5.27
BPT	5.24	-11.89
BPTF	5.20	-11.81
BPTCl	4.50	-10.24
BPTBr	2.15	-4.89
BPTI	5.29	-12.03

BPTI film persistence

In the Nyquist diagram in Fig. 13, some experimental curves with different immersion times can be observed. It can be seen that on day one, a maximum value of Z_{re} of approximately 800 Ω cm^2 is reached. Later, this value decreased by 50% and was stable until day 14 [56]. This is attributed to a dynamic adsorption-desorption process on the metallic surface. However, this process is not so fast because the Z_{re} value is higher than 200 Ω cm^2, and for comparison, the value of the blank is only 30 Ω cm^2 [57]. Moreover, the electrolyte begins to penetrate the inhibitor film to attack the metal surface [58].

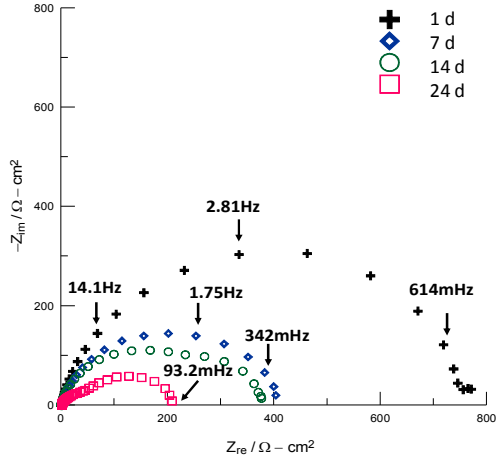

Fig. 13 Nyquist diagram for 50 ppm of BPTI as a function of the immersion time.

RSC Advances

ARTICLE

For greater clarity of the obtained inhibition efficiency, Fig. 14 shows the behaviour for long immersion times. It is observed that BPTI as a corrosion inhibitor shows good protection against corrosion with a η > of 80%, even after 504 hours of immersion.

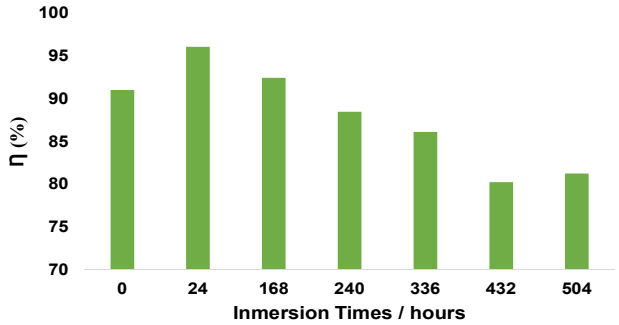

Fig. 14 Variation of the inhibition efficiency of BPTI with varying immersion times.

Rotation velocity effect (laminar flow)

After observing the BPTI corrosion inhibition, it was evaluated under hydrodynamic conditions using the same sweep of concentrations.

The results after adjustment of the electric circuit are shown in Fig. 15 and Table 5, where it can be noticed that the charge transference resistance value increased when the inhibitor concentration at both rotation velocities increased, and consequently, the inhibition efficiency value also increased.

Nevertheless, acceptable efficiencies are obtained at approximately 200 ppm (approximately 80%), and thus, this flow dynamic causes this parameter to be affected by a desorption phenomenon at these rotation velocities [59].

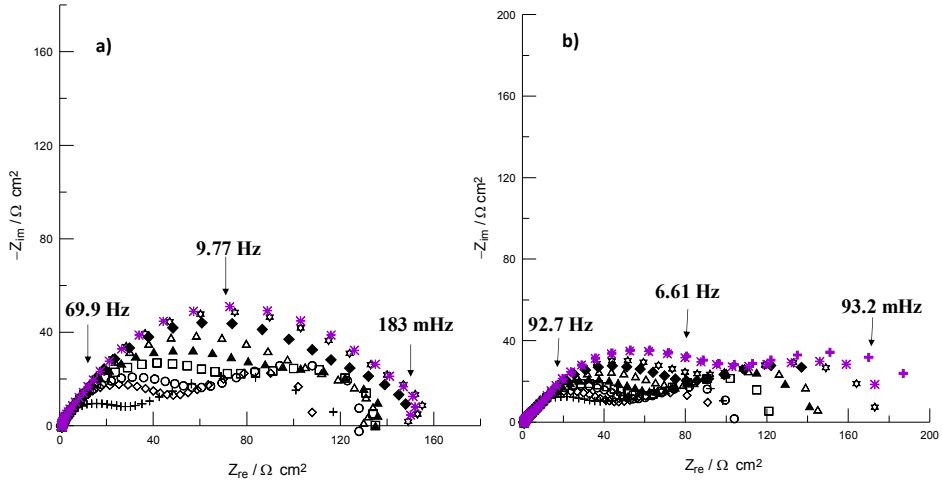

Fig. 15 Nyquist diagram of the concentration of BPTI in relation to the rotation velocities a) 300 rpm and b) 600 rpm on API 5L X52 steel in 1 M HCl.

Table 5 BPTI electrochemical parameters at different concentrations and rotation velocities.

	Rotation rate / rpm			
	300		600	
C ppm	R_{ct} Ω cm^2	η %	R_{ct} Ω cm^2	η %
5	89.0	66.3	79	58
10	65.3	54.1	70	57
15	72.0	58.3	58	48
20	70.7	57.5	71	58
25	122.0	75.4	73	59
30	123.4	75.7	85	65
50	137.5	78.2	98	70
100	144.6	79.3	125	76
200	160.8	81.3	134	78

SEM analysis

In Fig. 16, photographs obtained by SEM of the API 5L X52 steel surface are shown. The steel was polished and later immersed in 1 M HCl for 24 hours with and without BPTI inhibitor at 50 ppm

Comparing Figs. 16a and 16b, the latter shows strong damage on its surface without the presence of the inhibitor. Nevertheless, Fig. 16c shows how the BPTI inhibitor has surface protective properties, revealing that the protective film is responsible for diminishing the damage caused.

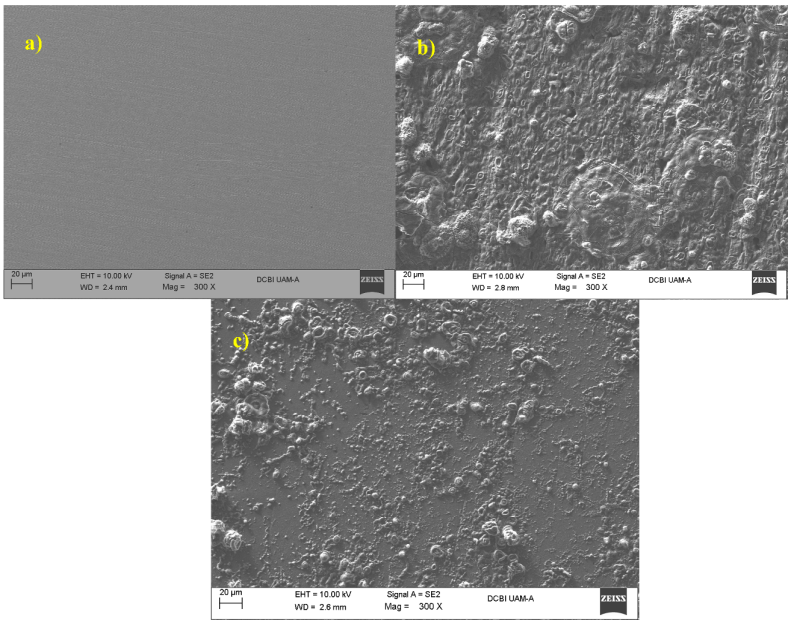

Fig. 16 SEM micrographs of API 5L X52 steel samples: a) polished, immersed in 1 M HCl, b) without inhibitor and c) in the presence of BPTI.

By means of chemical analysis (see Fig. 17), it was demonstrated that corrosive species (oxygen and chloride ions) quantitatively decrease in the presence of the BPTI inhibitor.

RSC Advances

ARTICLE

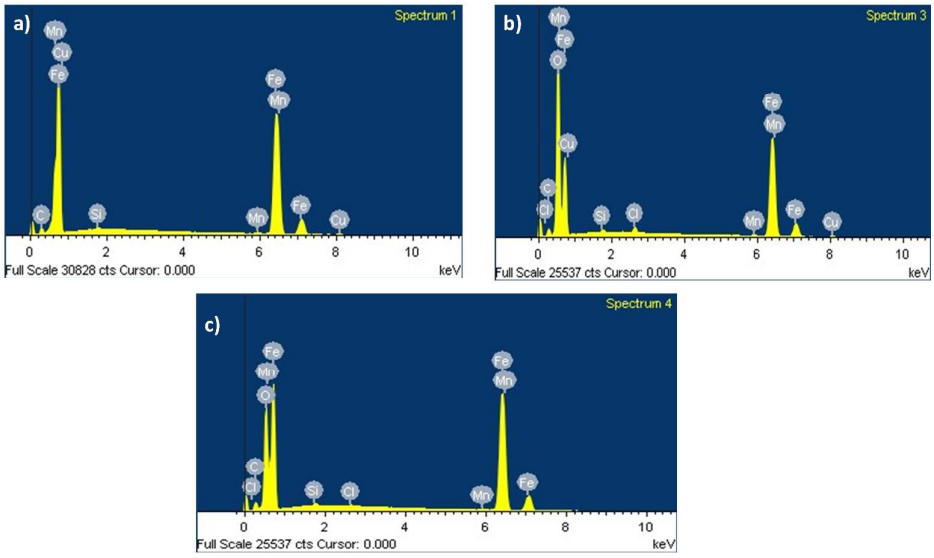

Fig. 17 API 5L X52 steel chemical analysis for the following samples: a) polished, immersed in 1 M HCl, b) without inhibitor and c) in the presence of BPTI.

Adsorption Mechanism

In acid solutions, the organic inhibitors have the ability of forming a protective film on the surface and the adsorption is determined by an electrostatic interaction (various active sites) between steel and inhibitor [60, 61].

The inhibition mechanism was proposed involving BPT´s inhibitor on metal surface:

(a) As a result of electrostatic interaction, the protonated BPT´s molecules (Fig. 18) are attracted toward the solid/liquid interface to form a protective film, preventing the metal from touching the aggressive medium.

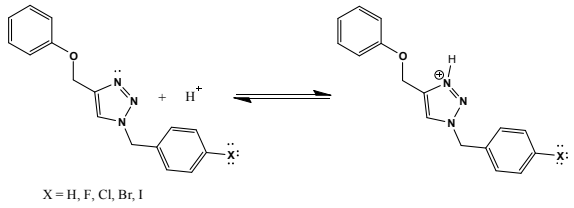

Fig. 18 Protonated Molecules of BPT´s in acidic solution

It is well known that the chloride ions have a small degree of hydration, and due to specific adsorption, they bring an excess negative charge toward the solution side of metal attracting most of the cations [62, 63].

(a) After the release of H_2 gas, cationic form of inhibitor molecules returns to its neutral form and the heteroatoms with free lone pair electrons promote chemical adsorption.

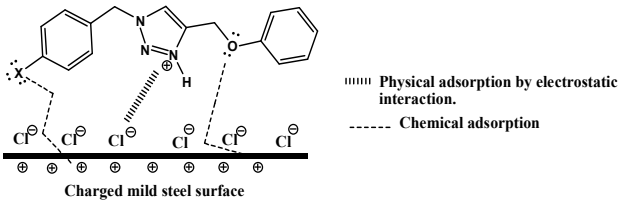

Fig. 19 Schematic adsorption mode of BPT´s on mild steel surface in 1M HCl.

On another hand, the halides ions are good ligands because exhibit low electronegativity (less than 3.5) except Fluoride ion. The electronegativity decreases from Cl to I (Cl = 3, Br = 2.8 and I=2.5) and the atomic radius (Cl = 0.90°A, Br = 1.14 °A and I=1.35°A). The inhibition effect increases in the order Cl < Br < I which seems to indicate that the radio and electronegativity of halogens ions may be have an important role to play [64].

In this study, the BPTI is the best corrosion inhibitor because the iodine atom has a large atomic radius and low electronegativity.

CONCLUSIONS

Phenol shows corrosion protection at concentrations higher than 50 ppm, and m

The corrosion inhibition of triazoles derived from phenol determined by electrochemical impedance spectroscopy follow the order:

BPTI > BPTBr > BPTCl > BPTF> BPT

The values of the Gibbs adsorption energy suggest that the interaction between the inhibitor and the metallic surface is of the physisorption type according to the Langmuir model.

The best inhibitor (BPTI) showed proper protection for long immersion times up to 336 hours with a η value of approximately 87%.

ACKNOWLEDGEMENTS

The authors would like to thank the Consejo Nacional de Ciencia y Tecnología, CONACyT (project 181448) for its financial support. We also wish to acknowledge the SNI (Sistema Nacional de Investigadores) for the distinction of their membership and the stipend received.

AEV and FJRG express their gratitude to the School of Chemistry (UNAM), Department of Metallurgy and DGAPA for providing a postdoctoral fellowship.

We thank the Divisional Electronic Mycroscopy Lab (Laboratorio Divisional de Microscopía Electrónica) for the use of SUPRA 55 VP.

Notes and references

1 P.Singh, V. Srivastava, M.A. Qaraishi, *J. Mol. Liq.,* 2016, **216,** 164.
2 T. K. Chaitra, K. N. Shetty, H. C. Tandon., *J. Mol. Liq.*, 2015, **211,** 1026.
3 M. Yadav, S. Kumar, R.R. Sinha, I. Bahadur, E.E. Ebenso, *J. Mol. Liq,* 2015, **211**, 135.
4 M. S. Shihab, H. H. Al-Doori, *J. Mol. Struc.,* 2014, **1076**, 658.
5 A. Yurt, B. Duran, H. Dal, *Arab. J. Chem., 2014,* **7,** 732.
6 F. Bisceglie, G. Del Monte, P. Tarasconi, G. Pelosi, *Inorg. Chim. Acta*, 2015, **434**, 143.
7 J. Saranya, P. Sounthari, K. Parameswari, S. Chitra, 2016, **77**, 175.
8 M.R. Noor El-Din, E.A. Khamis, *J. Ind. Eng. Chem.,* 2015*,* **24**, 342.
9 H. Hamani, T. Douadi, M. Al-Noaimi, S. Issaadi, D. Daoud, S. Shafaa, *Corros. Sci*., 2014, **88**, 234.
10 I. Lozano, E. Mazario, C.O. Olivares-Xometl, N.V. Likhanova, P. Herrasti, *Mater. Chem. Phys.,* 2014*,* **147** (1–2) 191.
11 C. Verma, M.A. Quraishi, A. Signh, *J. Mol. Liq.,* 2015*,* 212, 804.
12 L. O. Olasunkanmi, M. M. Kabanda, E. E. Ebenso, *Physica E: Low-dimensional Systems and Nanostructures,* 2016, **76**, 109.
13 M. Mobin, S. Zehra, M. Parveen, *J. Mol. Liq.,* 2016*,* **216**, 598.
14 A.M. Al-Sabagh, N.Gh. Kandile, N.M. Nasser, M.R. Mishrif, A. E. El-Tabey, *Egypt. J. of Pet.,* 2013, **22**(3), 351.
15 S. Ghareba, S. Omanovic, *Corros. Sci*., 2011, **53**, 3805.
16 E. Barmatov, T. Hughes, M. Nagl, *Corros. Sci.,* 2015, **92**, 85.
17 E E. Barmatov, T. Hughes, M. Nagl, *Corros. Sci.,* 2015, **92**, 85.
18 A. Kosari, M.H. Moayed, A. Davoodi, R. Parvizi, M. Momeni, H. Eshghi, H. Moradi, *Corros. Sci.,* 2014, **78**, 138.
19 S. Ghareba, S. Omanovic, *Corros. Sci*., 2011, **53**, 3805.
20 P. Bommersbach, C. Alemany-Dumont, J. Millet, B. Normand, *Electrochim. Act.,* 2006*,* **51,** 4011.
21 H. Ashassi-Sorkhabi, E. Asghari, Electrochim*. Act*., 2008, **54,** 162.
22 J. Liang, A. Deng, R. Xie, M. Gomez, J. Hu, J. Zhang, C. Nam Ong, A. Adin, *Desalination,* 2013, **322,** 76.
23 Q. Deng, N.-N. Ding, X.-L. Wei, L. Cai, X.-P. He, Y.-T. Long, G.-R. Chen, K. Chen, *Corros. Sci.,* 2012, **64,** 64.
24 Q. Deng, H.-W. Shi, N.-N. Ding, B.-Q. Chen, X.-P. He, G. Liu, Y. Tang, Y.-T. Long, G.-R. Chen, *Corros. Sci.,* 2012, **57,** 220.
25 H.-L.Zhang, X.-P. He, Q. Deng, Y.-T. Long, G.-R. Chen, K. Chen, *Carbohyd. Res*., 2012, **354**, 32.
26 Q. Deng, X.-P. He, H.-W. Shi, B.-Q. Chen, G. Liu, Y. Tang, Y.-T. Long, G.-R. Chen, K. Chen. *Ind. Eng. Chem. Res*., 2012, **51**, 7160.
27 T. Zhang, S. Cao, H. Quan, Z. Huang, S. Xu, *Res. Chem. Intermed*., 2015, **41**, 2709.
28 B. Ramaganthan, M. Gopiraman, L.O. Olasunkanmi, M.M. Kabanda, S. Yesudass, I. Bahadur, A.S. Adekunle, I.B. Obot, E.E. Ebenso, *RSC Adv*., 2015, **5**, 76675.
29 M. Meldal, C.W. Tornøe, *Chem. Rev.*, 2008, **108**, 2952.
30 J.E. Hein, V.V. Fokin, *Chem. Soc. Rev*., 2010, **39**, 1302.
31 G. E. Negrón-Silva, R. González-Olvera, D. Angeles-Beltrán, N. Maldonado-Carmona, A. Espinoza-Vázquez, M.E. Palomar-Pardavé, M.A. Romero-Romo, R. Santillan, *Molecules*, 2013, **18**, 4613.
32 R. González-Olvera, A. Espinoza-Vázquez, G. E. Negrón-Silva, M.E. Palomar-Pardavé, M. A. Romero-Romo, R. Santillan, Molecules*,* 2013, **18**, 15064.
33 A. Espinoza-Vázquez, G. E. Negrón-Silva, R. González-Olvera, D. Angeles-Beltrán, H. Herrera-Hernández, M. Romero-Romo, M.E. Palomar-Pardavé, *Mater. Chem. Phys*., 2014, **145**, 407.
34 D. Y. Cruz-Gonzalez, R. González-Olvera, G. E. Negrón-Silva, L. Lomas-Romero, A. Gutiérrez-Carrillo, M.E. Palomar-Pardavé, M. A. Romero-Romo, R. Santillan, J. Uruchurtu, *Synthesis,* 2014, **46**, 1217.
35 R. González-Olvera, V. Román-Rodríguez, G.E. Negrón-Silva, A. Espinoza-Vázquez, F.J. Rodríguez-Gómez, R. Santillan, *Molecules,* 2016, **21**, 250.
36 D. Mendoza-Espinosa, G. E. Negrón-Silva, L. Lomas-Romero, A. Gutiérrez-Carrillo, D. Soto-Castro, *Synthesis,* 2013, **45**, 2431.
37 M. P. Chakravarthy, K. N. Mohana, C. B. Pradeep Kumar and A. M. Badiea, *Am. Chem. Sci. J.*, 2015, **8**, 1.
38 W. A. Gayed, N. H. El Sayed, *Eur. J. Chem*., 2014, **5**, 563.
39 R. Álvarez-Bustamante, G. Negrón-Silva, M. Abreu-Quijano, H. HerreraHernández, M. Romero-Romo, A. Cuán, M. Palomar-Pardavé. *Electrochim. Acta,* 2009, **54**, 5393.
40 A. Popova, M. Christov, A. Zwetanova. *Corros. Sci.,* 2007, **49**, 2131.
41 A. Espinoza, G. Negrón, D. Angeles, M. E. Palomar, M. Romero, H. Herrera, *ECS Trans.,* 2011, **36** (1), 207.
42 A. Espinoza-Vázquez, G.E. Negrón-Silva, D. Angeles-Beltrán, H. Herrera-Hernández, M.E. Palomar-Pardavé, M.A. Romero-Romo. *Inter. J. Electrochem. Sci*., 2014, **9**, 493.
43 M. Tourabi, K. Nohair, M. Traisnel, C. Jama, F. Bentiss, *Corros. Sci.,* 2013, **75**, 123.
44 P. C. Okafor, X. Liu, Y. G. Zheng*, Corros. Sci*., 2009, **51**, 761.
45 B.V. Appa Rao, K. Chaitanya Kumar*, J. Mater. Sci. Technol*., 2014, 30, 65.
46 O. Ghasemi, I. Danaee, G. R. Rashed, M. Rashvandavei, M. H. Maddahy, J*. Cent. Soth Univ.*, 2013, **20**, 301.

47 S. Rameshkumar, 1: Danaee, M. RashvandAvei, M. Vijayan, *J. Mol. Liq*., 2015, **212**, 168.
48 N. Kumar, C.Verma, M.A. Quraishi, A. K. Mulherjee, *J. Mol. Liq.,* 2016, **215**, 47.
49 S. Shaban, A. Abd-Elaal, S. Tawfik*, J. Mol. Liq*., 2016, **216**, 392.
50 L. Muralana, M. Kabanda, E. Ebenso, *J. Mol. Liq*., 2016, **215**, 763.
51 T. K. Chaitra, K. N. Shetty Mohana, H. C. Tandon, *J. Mol. Liq*., 2015, **211**, 1026.
52 M. Lebrini, M. Traisnel, M. Lagrenée, B. Mernari, F. Bentiss, *Corros. Sci*., 2008, **50**, 473.
53 S. Zhang, Z. Tao, W. Li, B. Hou, *Appl. Surf. Sci.,* 2009, **255**, 6757.
54 K.R. Ansari, M.A. Quraishi, Ambrish Singh, *Corros. Sci*., 2014, **79**, 5.
55 D. M. Gurudatta, K. N. Mohanaa, H. C. Tando, *J. Mol. Liq*., 2015, **211**, 275.
56 H. Zhang, X. Pang, M. Zhou, C. Liu, L. Wei, K. Gao, *Appl. Surf. Sci*., 2015, **356**, 63.
57 I. Lozano, E. Mazario, C.O. Olivares-Xometl, N.V. Likhanova, P. Herrasti, *Mater. Chem. Phys*., 2014, **147**, 191.
58 A.M. Badiea, K.N. Mohana, *Corros. Sci*., 2009, **51**, 2231.
59 A. Espinoza, S. García, F. J. Rodríguez, *J. Anal. Bional. Tech*., 2015, **6**(6), 273.
60 G. Karthik, M. Sundaravadivelu, P. Rajkumar, *Res Chem Intermed,* 2015, **41**,1543
61 M. Farsak, H. Keles, M. Keles, *Corros. Sci.*, 2015, **98**, 223
62 N. Caliskan, Esvet Akbas, Mat. Chem. and Phys., 2011, **126,** 983
63 Gh. Golestani, M. Shahidi, D. Ghazanfari, Appl. Surf. Sci., 2014, **308,** 347
64 E.E Ebenso, *Mat. Chem and Phys*., 2003, **79**, 58.

TABLE OF CONTENTS ENTRY

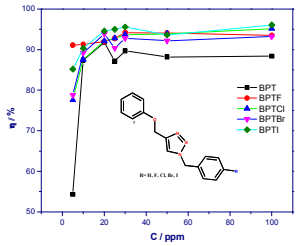

The phenol-derived triazoles beginning at 10 ppm show excellent inhibition against corrosion when immersed in 1 M HCl.